

# Electromagnetic Scattering by Surfaces of Arbitrary Shape

SADASIVA M. RAO, DONALD R. WILTON, SENIOR MEMBER, IEEE, AND ALLEN W. GLISSON, MEMBER, IEEE

**Abstract**—The electric field integral equation (EFIE) is used with the moment method to develop a simple and efficient numerical procedure for treating problems of scattering by arbitrarily shaped objects. For numerical purposes, the objects are modeled using planar triangular surfaces patches. Because the EFIE formulation is used, the procedure is applicable to both open and closed surfaces. Crucial to the numerical formulation is the development of a set of special subdomain-type basis functions which are defined on pairs of adjacent triangular patches and yield a current representation free of line or point charges at subdomain boundaries. The method is applied to the scattering problems of a plane wave illuminated flat square plate, bent square plate, circular disk, and sphere. Excellent correspondence between the surface current computed via the present method and that obtained via earlier approaches or exact formulations is demonstrated in each case.

## I. INTRODUCTION

ENGINEERS AND researchers in electromagnetics have been quick to take advantage of the expanding capabilities of digital computers over the past two decades by developing effective numerical techniques applicable to a wide variety of practical electromagnetic radiation and scattering problems. As new computer developments dramatically increase computational capabilities, however, it becomes less cost effective to develop highly efficient but specialized codes for treating certain classes of geometries than to use less efficient but existing general purpose codes that can handle a wide variety of problems. For these reasons there has been a growing interest in the use and development of computer codes for treating scattering by arbitrarily shaped conducting bodies.

To date, the most notable approaches for treating such problems have used integral equation formulations in conjunction with the method of moments. The body surface in these approaches is generally modeled either as a wire mesh—the so-called wire-grid model—or as a surface partitioned into smooth or piecewise-smooth patches—the so-called surface patch model.

The wire-grid modeling approach has been remarkably successful in treating many problems, particularly in those requiring the prediction of far-field quantities such as radiation patterns and radar cross sections [1]. Not only is the connectivity of a wire-grid model easily specified for computer input, but the approach also has the advantage that all numerically computed integrals in the moment matrix are one dimensional.

Manuscript received May 28, 1980; revised August 6, 1981. This work was supported by the Rome Air Development Center, Griffiss AFB, NY, under Contract No. F30602-78-C-0148.

S. M. Rao was with Syracuse University, Syracuse, NY, on leave from the Department of Electrical Engineering, University of Mississippi, University, MS 38677. He is now with the Department of Electrical Engineering, Rochester Institute of Technology, Rochester, NY 14623.

D. R. Wilton was with Syracuse University, Syracuse, NY, on leave from the Department of Electrical Engineering, University of Mississippi, University, MS 38677.

A. W. Glisson is with the Department of Electrical Engineering, University of Mississippi, University, MS 38677.

However, the approach is not well suited for calculating near-field and surface quantities such as surface current and input impedance. Some of the problems encountered include the presence of fictitious loop currents in the solution, ill-conditioned moment matrices and incorrect currents at the cavity resonant frequencies of the scatterer [2], and difficulties in interpreting computed wire currents and relating them to equivalent surface currents. The accuracy of wire-grid modeling has also been questioned on theoretical grounds [3]. Most of these difficulties can be either wholly or partially overcome by surface patch approaches, however, which account for much of the recent activity in this area.

Several approaches to surface patch modeling have been reported in the literature. Knepp and Goldhirsh [4] partitioned a conducting surface into nonplanar quadrilateral patches and employed the magnetic field integral equation (MFIE) to solve the electromagnetic scattering problem. Albertsen *et al.* [5] solved for the current and computed radiation patterns for satellite structures with attached wire antennas, booms, and solar panels. They employed a hybrid formulation in which the MFIE, with planar quadrilateral surface patches, was used to model the satellite, and the electric field integral equation (EFIE) was used to treat the wire antennas. Their approach also forms the basis for the arbitrary surface treatment of the widely used numerical electromagnetic code (NEC) developed at the Lawrence Livermore Laboratory [6]. Wang *et al.* [7] used an EFIE formulation and modeled relatively complex surfaces by means of planar rectangular patches. Newman and Pozar [8] extended the use of the well-known piecewise-sinusoidal basis functions of thin-wire theory to the treatment of surfaces in their EFIE formulation for surfaces with attached wires. Sankar and Tong [9] employed planar triangular patches to model a square plate and pointed out the possibility of extending their approach to arbitrary bodies. Their formulation, based on a variational formula for the current made stationary with respect to a set of trial functions, is equivalent to a Galerkin solution of the EFIE. Wang [10], [11] employed planar triangular patches in conjunction with the MFIE, but used basis functions containing the phase variation of the incident field in each patch, which unfortunately yield a moment matrix dependent on the incident field. Jeng and Wexler [12] suggested using the MFIE and nonplanar triangles to model arbitrary surfaces, while Singh and Adams [13] proposed the use of planar quadrilateral patches and sinusoidal basis functions in conjunction with the EFIE for the same purpose.

In arbitrary surface modeling the EFIE has the advantage of being applicable to both open and closed bodies, whereas the MFIE applies only to closed surfaces. On the other hand, for arbitrarily shaped objects the EFIE is considerably more difficult to apply than the MFIE. In fact, of the above authors, only Wang *et al.* and Newman and Pozar have actually applied the EFIE to nonplanar structures—and the use of rectangular patches limits their approaches to structures with curvature in one dimension only.

The difficulties with the EFIE stem primarily from the presence of derivatives appearing in conjunction with a singular kernel in the integral equation. For example, if the vector basis functions which represent the surface current are not constructed so that their normal components are continuous across surface edges, then the continuity equation demands the presence of line or point charges at such edges. These fictitious charges, when present, usually cause anomalies or inconsistencies in the solution. Although the approaches of Wang *et al.* and Newman and Pozar are free of these difficulties, their use of rectangular patches, with their consequent limitation to surfaces with curvature in one dimension only, is too restrictive for many applications.

For modeling arbitrarily shaped surfaces, planar triangular patch models, an example of which is shown in Fig. 1, are particularly appropriate. Some of the advantages of triangular patch surface modeling have been noted by Sankar and Tong [9], as well as by Wang [10], and are similar to those of wire-grid modeling. For example, triangular patches are capable of accurately conforming to any geometrical surface or boundary, the patch scheme is easily specified for computer input, and a varying patch density can be used according to the resolution required in the surface geometry or current. Although planar quadrilateral (nonrectangular) patches share some of these features, it is difficult to construct basis functions defined on them which are free of line charges. Furthermore, the vertices of planar quadrilaterals cannot be independently specified—a restriction that is a severe inconvenience to the modeler.

In this paper, a numerical solution of the problem of scattering by either open or closed arbitrarily shaped conducting bodies is presented. The approach combines the advantages of triangular patch modeling and the EFIE formulation, and results in an algorithm which is both simple and efficient. Crucial to the approach is the development of special basis functions defined on triangular patches which are free of fictitious line or point charges and which are analogous to the so-called "roof-top" functions used in rectangular patch models [14].

In the following section the EFIE formulation is presented, the special set of basis functions is developed, and the method of moments [15] is applied to obtain a linear system of equations for the surface current. In Section III, numerical results are presented for scattering by a flat square plate, a bent square plate, a circular disk, and a sphere. Section IV summarizes the contents of the paper.

## II. ELECTRIC FIELD FORMULATION

In this section an integral equation for the surface current induced on a conducting scatterer is derived from boundary conditions on the electric field. To solve the integral equation by the method of moments, a set of expansion functions and a testing procedure are developed and used to derive the elements of the moment matrix. Finally, the numerical computation of the moment matrix elements is discussed.

### *Electric Field Integral Equation*

Let  $S$  denote the surface of an open or closed perfectly conducting scatterer with unit normal  $\hat{\mathbf{n}}$ . An electric field  $\mathbf{E}^i$ , defined to be the field due to an impressed source in the absence of the scatterer, is incident on and induces surface currents  $\mathbf{J}$  on  $S$ . If  $S$  is open, we regard  $\mathbf{J}$  as the vector sum of the surface currents on opposite sides of  $S$ ; hence the normal component of  $\mathbf{J}$  must vanish on boundaries of  $S$ . The scattered electric field

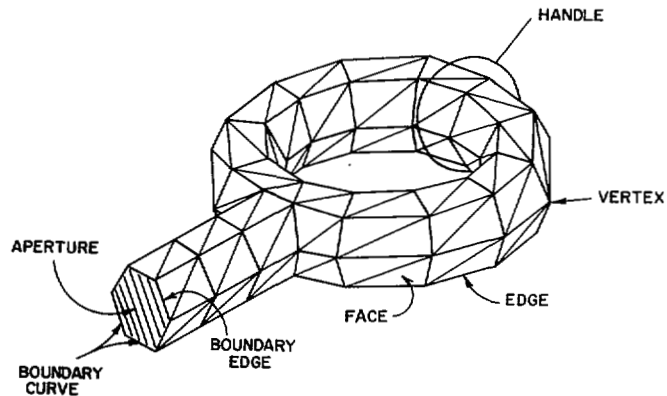


Fig. 1. Arbitrary surface modeled by triangular patches.

$\mathbf{E}^s$  can be computed from the surface current by

$$\mathbf{E}^s = -j\omega\mathbf{A} - \nabla\Phi \quad (1)$$

with the magnetic vector potential defined as

$$\mathbf{A}(\mathbf{r}) = \frac{\mu}{4\pi} \int_S \mathbf{J} \frac{e^{-jkR}}{R} dS' \quad (2)$$

and the scalar potential as

$$\Phi(\mathbf{r}) = \frac{1}{4\pi\epsilon} \int_S \sigma \frac{e^{-jkR}}{R} dS'. \quad (3)$$

A harmonic time dependence  $\exp(j\omega t)$  is assumed and suppressed, and  $k = \omega\sqrt{\mu\epsilon} = 2\pi/\lambda$ , where  $\lambda$  is the wavelength. The permeability and permittivity of the surrounding medium are  $\mu$  and  $\epsilon$ , respectively, and  $R = |\mathbf{r} - \mathbf{r}'|$  is the distance between an arbitrarily located observation point  $\mathbf{r}$  and a source point  $\mathbf{r}'$  on  $S$ . Both  $\mathbf{r}$  and  $\mathbf{r}'$  are defined with respect to a global coordinate origin  $\hat{O}$ . The surface charge density  $\sigma$  is related to the surface divergence of  $\mathbf{J}$  through the equation of continuity,

$$\nabla_s \cdot \mathbf{J} = -j\omega\sigma. \quad (4)$$

We derive an integrodifferential equation for  $\mathbf{J}$  by enforcing the boundary condition  $\hat{\mathbf{n}} \times (\mathbf{E}^i + \mathbf{E}^s) = \mathbf{0}$  on  $S$ , obtaining

$$-\mathbf{E}_{\tan}^i = (-j\omega\mathbf{A} - \nabla\Phi)_{\tan}, \quad \mathbf{r} \text{ on } S. \quad (5)$$

Equation (5), with (2)–(4), constitutes the so-called electric field integral equation. One notes that the presence of derivatives on the current in (4) and on the scalar potential in (5) suggests that care should be taken in selecting the expansion functions and testing procedure in the method of moments.

### *Development of Basis Functions*

In this section we discuss a set of basis functions introduced by Glisson [16] which is suitable for use with the EFIE and triangular patch modeling. We assume that a suitable triangulation, defined in terms of an appropriate set of faces, edges, vertices, and boundary edges, as illustrated in Fig. 1, has been found to approximate  $S$ . (More detailed considerations concerning the mathematical representation and topological properties of triangular patch models may be found in [17].)

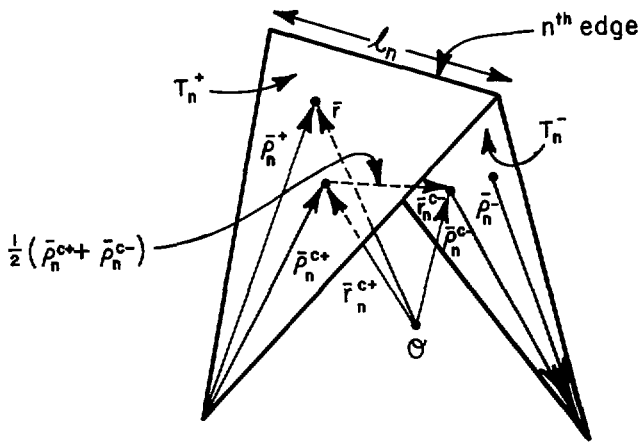


Fig. 2. Triangle pair and geometrical parameters associated with interior edge.

It is convenient to start our development by noting that each basis function is to be associated with an *interior edge* (i.e., nonboundary edge (cf Fig. 1)) of the patch model and is to vanish everywhere on  $S$  except in the two triangles attached to that edge. Fig. 2 shows two such triangles,  $T_n^+$  and  $T_n^-$ , corresponding to the  $n$ th edge of a triangulated surface modeling a scatterer. Points in  $T_n^+$  may be designated either by the position vector  $\mathbf{r}$  defined with respect to  $O$ , or by the position vector  $\rho_n^+$  defined with respect to the free vertex of  $T_n^+$ . Similar remarks apply to the position vector  $\rho_n^-$  except that it is directed toward the free vertex of  $T_n^-$ . The plus or minus designation of the triangles is determined by the choice of a positive current reference direction for the  $n$ th edge, the reference for which is assumed to be from  $T_n^+$  to  $T_n^-$ .<sup>1</sup> We define the vector basis function associated with the  $n$ th edge as

$$\mathbf{f}_n(\mathbf{r}) = \begin{cases} \frac{l_n}{2A_n^+} \rho_n^+, & \mathbf{r} \text{ in } T_n^+ \\ \frac{l_n}{2A_n^-} \rho_n^-, & \mathbf{r} \text{ in } T_n^- \\ \mathbf{0}, & \text{otherwise,} \end{cases} \quad (6)$$

where  $l_n$  is the length of the edge and  $A_n^\pm$  is the area of triangle  $T_n^\pm$ . (Note that we use the convention, followed throughout the paper, that subscripts refer to edges while superscripts refer to faces.) The basis function  $\mathbf{f}_n$  is used to approximately represent the surface current, and we list and discuss below some properties which make it uniquely suited to this role.

- 1) The current has no component normal to the boundary (which excludes the common edge) of the surface formed by the triangle pair  $T_n^+$  and  $T_n^-$ , and hence no line charges exist along this boundary.
- 2) The component of current normal to the  $n$ th edge is constant and continuous across the edge as may be seen

<sup>1</sup> For orientable surfaces, the current reference direction may be obtained from the connection matrix used to describe the triangulation scheme. This matrix merely lists the vertices linked by each edge, the order of appearance of the vertices for each edge effectively assigning an orientation to the edge. The direction of the cross product of this edge orientation vector with the surface normal in each adjacent triangle may be taken as the positive current reference direction in that triangle for the basis function associated with the edge.

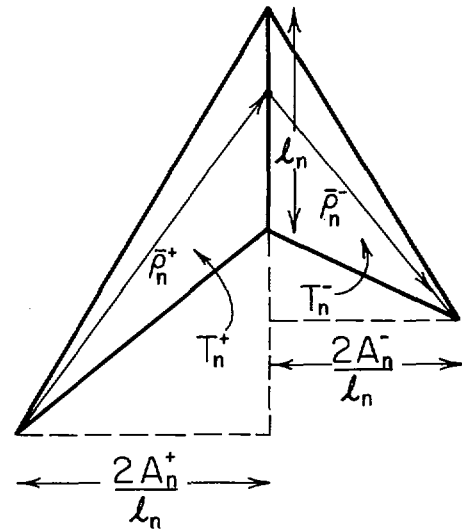


Fig. 3. Geometry for construction of component of basis function normal to edge.

with the aid of Fig. 3, which shows that the normal component of  $\rho_n^\pm$  along edge  $n$  is just the height of triangle  $T_n^\pm$  with edge  $n$  as the base and the height expressed as  $(2A_n^\pm)/l_n$ . This latter factor normalizes  $\mathbf{f}_n$  in (6) such that its flux density normal to edge  $n$  is unity, ensuring continuity of current normal to the edge. This result, together with 1), implies that *all* edges of  $T_n^+$  and  $T_n^-$  are free of line charges.

- 3) The surface divergence of  $\mathbf{f}_n$ , which is proportional to the surface charge density associated with the basis element, is

$$\nabla_s \cdot \mathbf{f}_n = \begin{cases} \frac{l_n}{A_n^+}, & \mathbf{r} \text{ in } T_n^+ \\ -\frac{l_n}{A_n^-}, & \mathbf{r} \text{ in } T_n^- \\ 0, & \text{otherwise,} \end{cases} \quad (7)$$

since the surface divergence in  $T_n^\pm$  is  $(\pm 1/\rho_n^\pm) \partial(\rho_n^\pm \mathbf{f}_n) / \partial \rho_n^\pm$ . The charge density is thus constant in each triangle, the total charge associated with the triangle pair  $T_n^+$  and  $T_n^-$  is zero, and the basis functions for the charge evidently have the form of *pulse doublets* [14].

- 4) The *moment* of  $\mathbf{f}_n$  is given by  $(A_n^+ + A_n^-) \mathbf{f}_n^{\text{avg}}$  where

$$\begin{aligned} (A_n^+ + A_n^-) \mathbf{f}_n^{\text{avg}} &\equiv \int_{T_n^+ + T_n^-} \mathbf{f}_n dS \\ &= \frac{l_n}{2} (\rho_n^{c+} + \rho_n^{c-}) \\ &= l_n (\mathbf{r}_n^{c+} - \mathbf{r}_n^{c-}) \end{aligned} \quad (8)$$

and  $\rho_n^{c\pm}$  is the vector between the free vertex and the centroid of  $T_n^\pm$  with  $\rho_n^{c-}$  directed toward and  $\rho_n^{c+}$  directed away from the vertex, as shown in Fig. 2, and  $\mathbf{r}_n^{c\pm}$  is the vector from  $O$  to the centroid of  $T_n^\pm$ . Equation (8) may be most easily derived by expressing the

integral in terms of area coordinates, to be discussed below.

The current on  $S$  may be approximated in terms of the  $\mathbf{f}_n$  as

$$\mathbf{J} \cong \sum_{n=1}^N I_n \mathbf{f}_n(\mathbf{r}) \quad (9)$$

where  $N$  is the number of interior (nonboundary) edges. Since a basis function is associated with each nonboundary edge of the triangulated structure, up to three basis functions may have nonzero values within each triangular face. But at a given edge only the basis function associated with that edge has a current component *normal to the edge* since, according to 1), all other basis currents in adjacent faces are parallel to the edge. Furthermore, since the normal component of  $\mathbf{f}_n$  at the  $n$ th edge is unity, *each coefficient  $I_n$  in (9) may be interpreted as the normal component of current density flowing past the  $n$ th edge*. Also, we see that the basis functions are independent in each triangle since the current normal to the  $n$ th edge,  $I_n$  in (9), is an independent quantity. At surface boundary edges, the sum of the normal components of current on opposite sides of the surface cancel because of current continuity. Therefore we neither define nor include in (9) contributions from basis functions associated with such edges.

Because of the considerable variation in the direction of the flow lines of  $\mathbf{f}_n$  within a triangle, it is not at first obvious that a linear superposition of basis functions is capable of representing, say, a constant current flowing in an arbitrary direction within a triangle. That this is possible, however, can be seen with the aid of Fig. 4, which shows a triangle  $T^q$  with edges arbitrarily labeled 1, 2, and 3 (in effect, we employ here a "local indexing scheme," in contrast to the "global indexing scheme" used earlier). With the vectors  $\rho_1$ ,  $\rho_2$ , and  $\rho_3$  as shown, the basis functions in  $T^q$  are  $\mathbf{f}_i = (l_i/2A^q)\rho_i$ ,  $i = 1, 2, 3$ , where  $A^q$  is the triangle area and where, for simplicity, the current reference directions are assumed to be out of the triangle for each edge. It is apparent from the figure and the definition of  $\mathbf{f}_i$  that the linear combinations  $l_2\mathbf{f}_1 - l_1\mathbf{f}_2$  and  $l_3\mathbf{f}_1 - l_1\mathbf{f}_3$  are *constant* vectors for every point  $\mathbf{r}$  in  $T^q$  and are parallel to sides 3 and 2, respectively. Since the two composite forms are linearly independent (i.e., nonparallel), a constant vector of arbitrary magnitude and direction within  $T^q$  may be synthesized by an appropriate linear combination of the two forms, as asserted.

#### Testing Procedure

The next step in the method of moments is to select a testing procedure. We choose as testing functions the expansion functions  $\mathbf{f}_n$  developed in the previous section. With a symmetric product defined as

$$\langle \mathbf{f}, \mathbf{g} \rangle \equiv \int_S \mathbf{f} \cdot \mathbf{g} dS, \quad (10)$$

(5) is tested with  $\mathbf{f}_m$ , yielding

$$\langle \mathbf{E}^i, \mathbf{f}_m \rangle = j\omega \langle \mathbf{A}, \mathbf{f}_m \rangle + \langle \nabla \Phi, \mathbf{f}_m \rangle. \quad (11)$$

If one makes use of a surface vector calculus identity [18] and the properties of  $\mathbf{f}_m$  at the edges of  $S$ , the last term in (11) can

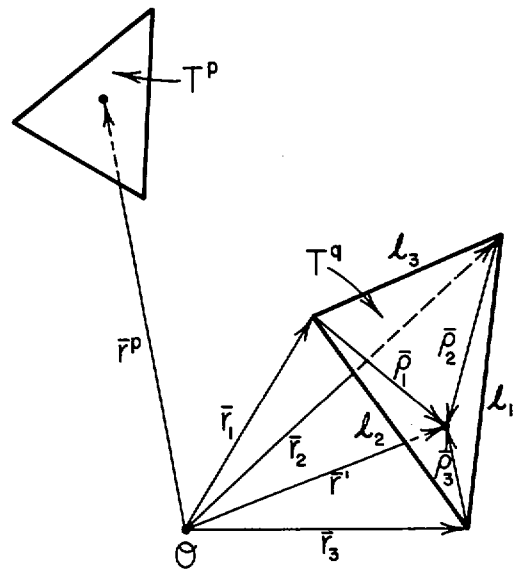


Fig. 4. Local coordinates and edges for source triangle  $T^q$  with observation point in triangle  $T^p$ .

be rewritten as

$$\langle \nabla \Phi, \mathbf{f}_m \rangle \cong - \int_S \Phi \nabla_s \cdot \mathbf{f}_m dS. \quad (12)$$

With (7), the integral in (12) may now be written and approximated as follows:

$$\begin{aligned} & \int_S \Phi \nabla_s \cdot \mathbf{f}_m dS \\ &= l_m \left( \frac{1}{A_m^+} \int_{T_m^+} \Phi dS - \frac{1}{A_m^-} \int_{T_m^-} \Phi dS \right) \\ &\cong l_m [\Phi(\mathbf{r}_m^{c+}) - \Phi(\mathbf{r}_m^{c-})]. \end{aligned} \quad (13)$$

In (13) the average of  $\Phi$  over each triangle is approximated by the value of  $\Phi$  at the triangle centroid. With similar approximations, the vector potential and incident field terms in (11) may be written as

$$\begin{aligned} & \left\langle \begin{Bmatrix} \mathbf{E}^i \\ \mathbf{A} \end{Bmatrix}, \mathbf{f}_m \right\rangle \\ &= l_m \left[ \frac{1}{2A_m^+} \int_{T_m^+} \begin{Bmatrix} \mathbf{E}^i \\ \mathbf{A} \end{Bmatrix} \cdot \rho_m^+ dS \right. \\ & \quad \left. + \frac{1}{2A_m^-} \int_{T_m^-} \begin{Bmatrix} \mathbf{E}^i \\ \mathbf{A} \end{Bmatrix} \cdot \rho_m^- dS \right] \\ &\cong \frac{l_m}{2} \left[ \begin{Bmatrix} \mathbf{E}^i(\mathbf{r}_m^{c+}) \\ \mathbf{A}(\mathbf{r}_m^{c+}) \end{Bmatrix} \cdot \rho_m^{c+} \right. \\ & \quad \left. + \begin{Bmatrix} \mathbf{E}^i(\mathbf{r}_m^{c-}) \\ \mathbf{A}(\mathbf{r}_m^{c-}) \end{Bmatrix} \cdot \rho_m^{c-} \right], \end{aligned} \quad (14)$$

where the integral over each triangle is eliminated by approximating  $\mathbf{E}^i$  (or  $\mathbf{A}$ ) in each triangle by its value at the triangle centroid and carrying out integrations similar to those used to obtain (8). With (12)-(14), (11) now becomes

$$\begin{aligned} & j\omega l_m \left[ \mathbf{A}(\mathbf{r}_m^{c+}) \cdot \frac{\rho_m^{c+}}{2} + \mathbf{A}(\mathbf{r}_m^{c-}) \cdot \frac{\rho_m^{c-}}{2} \right] \\ & + l_m [\Phi(\mathbf{r}_m^{c-}) - \Phi(\mathbf{r}_m^{c+})] \\ & = l_m \left[ \mathbf{E}^i(\mathbf{r}_m^{c+}) \cdot \frac{\rho_m^{c+}}{2} + \mathbf{E}^i(\mathbf{r}_m^{c-}) \cdot \frac{\rho_m^{c-}}{2} \right], \end{aligned} \quad (15)$$

which is the equation enforced at each triangle edge,  $m = 1, 2, \dots, N$ .

We remark that another interpretation of the testing procedure arriving at (15) is also possible. One may equate line integrals of the form  $\int_{C_m} \mathbf{F} \cdot d\mathbf{r}$ , where  $\mathbf{F}$  represents the right and left sides of (5), and  $C_m$  is the piecewise linear path from the point  $\mathbf{r}_m^{c+}$  to the midpoint of edge  $m$  and thence to  $\mathbf{r}_m^{c-}$ .  $\mathbf{E}^i$  and  $\mathbf{A}$  can be approximated along each portion of the path by their respective values at the triangle centroids. The resulting equality, apart from the factor  $l_m$ , is (15). Under either interpretation, the testing procedure reduces the differentiability requirement on  $\Phi$  in (5) by integrating  $\nabla\Phi$  first, the procedure having been constructed with this goal in mind. The purpose of approximations (13) and (14) is to eliminate surface integrals of the potential quantities, allowing a double surface integral to be approximated by a quantity involving a single surface integral in the numerical computation of the moment matrix elements. These approximations are justified by observing that the potentials are locally smooth within each subdomain, as follows from their integral definitions and the locally smooth nature of the source representation in terms of the basis functions [14].<sup>2</sup>

#### Matrix Equation Derivation

Substitution of the current expansion (9) into (15) yields an  $N \times N$  system of linear equations which may be written in matrix form as

$$\mathbf{Z}\mathbf{I} = \mathbf{V} \quad (16)$$

where  $\mathbf{Z} = [Z_{mn}]$  is an  $N \times N$  matrix and  $\mathbf{I} = [I_n]$  and  $\mathbf{V} = [V_m]$  are column vectors of length  $N$ . Elements of  $\mathbf{Z}$  and  $\mathbf{V}$  are given by

$$\begin{aligned} Z_{mn} = l_m \left[ j\omega \left( \mathbf{A}_{mn}^+ \cdot \frac{\rho_m^{c+}}{2} + \mathbf{A}_{mn}^- \cdot \frac{\rho_m^{c-}}{2} \right) \right. \\ \left. + \Phi_{mn}^- - \Phi_{mn}^+ \right] \end{aligned} \quad (17)$$

<sup>2</sup> Note that if the approximations (13) and (14) had not been made, the procedure leading to (15) would have been identical to Galerkin's method since the basis and testing functions chosen are identical [15]. For the EFIE, the matrix would then satisfy the symmetry property  $Z_{mn} = Z_{nm}$ , but this desirable property is lost due to the approximations made. Since  $Z_{mn}$  and  $Z_{nm}$  are different approximations to the same quantity, however, then their average also approximates the quantity, and one tempting possibility is to average  $\mathbf{Z}$  with its transpose, thus restoring the symmetry property to the moment matrix. This approach, however, has not to date been tested.

$$V_m = l_m \left( \mathbf{E}_m^+ \cdot \frac{\rho_m^{c+}}{2} + \mathbf{E}_m^- \cdot \frac{\rho_m^{c-}}{2} \right) \quad (18)$$

where

$$\mathbf{A}_{mn}^\pm = \frac{\mu}{4\pi} \int_S \mathbf{f}_n(\mathbf{r}') \frac{e^{-jkR_{m^\pm}}}{R_{m^\pm}} dS', \quad (19)$$

$$\Phi_{mn}^\pm = -\frac{1}{4\pi j\omega\epsilon} \int_S \nabla_{s'} \cdot \mathbf{f}_n(\mathbf{r}') \frac{e^{-jkR_{m^\pm}}}{R_{m^\pm}} dS', \quad (20)$$

$$R_{m^\pm} = |\mathbf{r}_m^{c^\pm} - \mathbf{r}'|$$

and

$$\mathbf{E}_m^\pm = \mathbf{E}^i(\mathbf{r}_m^{c^\pm}). \quad (21)$$

For plane wave incidence, we set

$$\mathbf{E}^i(\mathbf{r}) = (E_\theta \hat{\theta}_0 + E_\phi \hat{\phi}_0) e^{j\mathbf{k} \cdot \mathbf{r}} \quad (22)$$

where the propagation vector  $\mathbf{k}$  is

$$\begin{aligned} \mathbf{k} = k (\sin \theta_0 \cos \phi_0 \hat{\mathbf{x}} \\ + \sin \theta_0 \sin \phi_0 \hat{\mathbf{y}} + \cos \theta_0 \hat{\mathbf{z}}) \end{aligned} \quad (23)$$

and  $(\hat{\theta}_0, \hat{\phi}_0)$  defines the angle of arrival of the plane wave in terms of the usual spherical coordinate convention. Unit vectors  $\theta_0$  and  $\phi_0$  are *constant* vectors which coincide with the usual spherical coordinate unit vectors only at points on the line from  $O$  in the direction of  $\mathbf{k}$ .

Once the elements of the moment matrix and the forcing vector  $\mathbf{V}$  are determined, one may solve the resulting system of linear equations (16) for the unknown column vector  $\mathbf{I}$ . The elements of  $\mathbf{Z}$  in (16) may be evaluated by naively computing  $Z_{mn}$  directly by (17) (with aid of (19) and (20)) for each index combination  $m$  and  $n$ . However, as shown in the next section, this procedure is extremely inefficient since the integrals required for each combination of  $m$  and  $n$  are generally required for a number of other combinations as well.

#### Efficient Numerical Evaluation of Matrix Elements

Evaluation of each matrix element  $Z_{mn}$  associated with edges  $m$  and  $n$  involves integrations over triangles  $T_n^\pm$  with observation points located at the centroids of triangles  $T_m^\pm$ . One is easily convinced that some of the same integrals required for an element  $Z_{mn}$  are also needed to compute an element  $Z_{rs}$ ,  $r \neq m$ ,  $s \neq n$ , if edge  $r$  happens to be an edge of  $T_m^+$  or  $T_m^-$  while edge  $s$  is an edge of  $T_n^+$  or  $T_n^-$ . Indeed, if one focuses attention on a single pair of *faces* rather than on a pair of *edges*, one observes that the integrals evaluated for a source face with scalar and vector potentials observed at the centroid of another face are involved in all the elements  $Z_{mn}$  having edges  $n$  as (nonboundary) edges of the source triangle and edges  $m$  as the (nonboundary) edges of the observation triangle. Thus, the total number of matrix elements requiring evaluation of the same potential integrals can be as large as nine. Clearly then, it is far more efficient to compute the required potential integrals by face-pair combinations, rather

than directly compute single elements of  $Z$  by edge-pair combinations. For each face-pair combination, the potential integrals may be multiplied by the appropriate coefficients (cf (17)) and their contributions accumulated in the appropriate elements of  $Z$  as they are computed.

In accordance with the above discussion, consider the evaluation of the vector and scalar potential integrals for a given source and observation face combination. Fig. 4 illustrates such a face pair with an observation point in face  $p$  and with source currents residing in face  $q$ . Each of the three basis functions which may exist simultaneously in  $T^q$  is proportional to one of the vectors  $\rho_1$ ,  $\rho_2$ , or  $\rho_3$  defined in the figure. Each vector  $\rho_i$ ,  $i = 1, 2, 3$ , is shown directed away from its associated vertex in the figure, but would be directed toward the vertex if the current reference direction for the associated edge were into the triangle. Consequently,

$$\rho_i = \pm(\mathbf{r}' - \mathbf{r}_i), \quad i = 1, 2, 3, \quad (24)$$

where the positive sign is used if the positive current reference direction is out of  $T^q$  and the negative sign is used otherwise. We wish to evaluate the magnetic vector potential,

$$\mathbf{A}_i^{pq} = \frac{\mu}{4\pi} \int_{T^q} \left( \frac{l_i}{2A^q} \right) \rho_i \frac{e^{-jkR^p}}{R^p} dS', \quad (25)$$

and the electric scalar potential,

$$\Phi_i^{pq} = -\frac{1}{4\pi j\omega\epsilon} \int_{T^q} \left( \frac{l_i}{A^q} \right) \frac{e^{-jkR^p}}{R^p} dS', \quad (26)$$

associated with the  $i$ th basis function on face  $q$  observed at the centroid of face  $p$ . In (25) and (26),

$$R^p = |\mathbf{r}^{cp} - \mathbf{r}'| \quad (27)$$

where  $\mathbf{r}^{cp}$  is the position vector of the centroid of face  $p$ .

Integrals (25) and (26) are most conveniently evaluated by transforming from the global coordinate system to a local system of coordinates defined within  $T^q$ . To define these coordinates, note that the vectors  $\rho_i$  in Fig. 4 divide  $T^q$  into three subtriangles of areas  $A_1$ ,  $A_2$ , and  $A_3$ , with  $l_1$ ,  $l_2$ , and  $l_3$ , respectively, as one of their sides. The areas are not independent, however, since they must satisfy  $A_1 + A_2 + A_3 = A^q$ . We now introduce the so-called *normalized area coordinates* [19]

$$\xi = \frac{A_1}{A^q}, \quad \eta = \frac{A_2}{A^q}, \quad \zeta = \frac{A_3}{A^q}, \quad (28)$$

which, because of the area constraint, must satisfy

$$\xi + \eta + \zeta = 1. \quad (29)$$

Note that all three coordinates vary between zero and unity in  $T^q$  and that at the triangle corners  $\mathbf{r}_1$ ,  $\mathbf{r}_2$ , and  $\mathbf{r}_3$ , the triplet  $(\xi, \eta, \zeta)$  takes on the values  $(1, 0, 0)$ ,  $(0, 1, 0)$ , and  $(0, 0, 1)$ , respectively. The transformation from Cartesian to normalized area coordinates may be written in vector form as

$$\mathbf{r}' = \xi\mathbf{r}_1 + \eta\mathbf{r}_2 + \zeta\mathbf{r}_3, \quad (30)$$

where  $\xi$ ,  $\eta$ , and  $\zeta$  are subject to the constraint (29). It can easily

be shown that surface integrals over  $T^q$  transform as follows:

$$\int_{T^q} g(\mathbf{r}) dS = 2A^q \int_0^1 \int_0^{1-\eta} g[\xi\mathbf{r}_1 + \eta\mathbf{r}_2 + (1-\xi-\eta)\mathbf{r}_3] d\xi d\eta. \quad (31)$$

With (24), (27), (30), and (31), (25) and (26) may now be written as

$$\mathbf{A}_i^{pq} = \pm \frac{\mu l_i}{4\pi} (\mathbf{r}_1 I_\xi^{pq} + \mathbf{r}_2 I_\eta^{pq} + \mathbf{r}_3 I_\zeta^{pq} - \mathbf{r}_H^{pq}) \quad (32)$$

and

$$\Phi_i^{pq} = \mp \frac{l_i}{j2\pi\omega\epsilon} I^{pq}, \quad (33)$$

where

$$I^{pq} = \int_0^1 \int_0^{1-\eta} \frac{e^{-jkR^p}}{R^p} d\xi d\eta, \quad (34a)$$

$$I_\xi^{pq} = \int_0^1 \int_0^{1-\eta} \xi \frac{e^{-jkR^p}}{R^p} d\xi d\eta, \quad (34b)$$

$$I_\eta^{pq} = \int_0^1 \int_0^{1-\eta} \eta \frac{e^{-jkR^p}}{R^p} d\xi d\eta, \quad (34c)$$

$$I_\zeta^{pq} = I^{pq} - I_\xi^{pq} - I_\eta^{pq}. \quad (34d)$$

Thus only three independent integrals, (34a)–(34c), must be numerically evaluated for each combination of face pairs  $p$  and  $q$ . The three integrals, in turn, contribute to up to nine elements of  $Z$  in (16). For a closed object with  $N$  edges the number of independent integrals computed is  $4N^2/3$ . By contrast, the edge-by-edge approach would require the evaluation of  $12N^2$  integrals or nine times as many. Numerical evaluation of the integrals (34a)–(34c) may be accomplished by using numerical quadrature techniques specially developed for triangular domains [20]. However, for the terms in which  $p = q$  the integrands are singular, and for these cases the singular portion of each integrand must be removed and integrated analytically [17].

### III. NUMERICAL RESULTS

In this section numerical results are presented for surface current distributions induced on selected scatterers under plane wave illumination. Although one radar cross-section example is given, emphasis in the examples is on the calculation of current distributions, not only because of their practical value in problems such as electromagnetic compatibility and nuclear electromagnetic pulse (EMP) penetration, but also because we believe that the calculation of accurate surface currents is a much more stringent test of a numerical approach than is ultimate calculation of far-field quantities. The geometries considered are a conducting square plate, a bent plate, a circular disk, and a sphere. The plate and disk problems involve open surfaces and therefore are a test of the EFIE approach when edges are present. The disk also serves as an example of a structure with a curved boundary, while the sphere

exemplifies both a closed surface and a doubly curved surface. Both problems are examples of surfaces not amenable to rectangular patch modeling. A summary of the computational resources required to calculate results for several of the examples is given at the end of the section.

### Flat Plate

Figs. 5 and 6 show the dominant component current distributions along the two principal cuts on a square plate illuminated by a normally incident plane wave. For comparison, the solution of Glisson [16], obtained using rectangular patches, is also given. The number of patches listed in the figures refers to the number of *charge* patches in the earlier solution of Glisson and to the number of triangles (also equal to the number of charge patches) in the present solution. Note that these quantities play similar roles in the two approaches. No comparison of the convergence rate of the two approaches should be inferred from the figures since both solutions are already well converged for the number of unknowns used. Note also that the density of data points appearing in the figures for the triangular patch solution is not truly indicative of the linear density of the subdomains. This is because, in effect, we show data points only for every other edge, i.e., only for those edges where the current reference direction vector is parallel to the current component we wish to observe.

Fig. 5 shows the current induced on a plate  $0.15 \lambda$  on each side. At this low frequency the current distribution is largely determined by the edge conditions and hence this case provides a good test of the technique's capacity for handling surface edges. We note the absence of any anomalies in the computed distribution near the plate edges. The elimination of such anomalies is attributed to the use of basis functions in which the expansion coefficients are not associated with current components parallel to plate edges and to a testing procedure in which potentials are not evaluated at edges [14].

Fig. 6 shows corresponding results for a  $1.0 \lambda$  square plate. From the figure, one observes that the edge behavior of the current distribution is confined to a relatively smaller region near the edges than for the  $0.15 \lambda$  plate and that the current on the interior portion of the plate has begun to exhibit the physical optics-plus standing wave distribution characteristic of the higher frequencies. Also shown for comparison are the corresponding results reported in [21].<sup>3</sup> Note that because of the placement of subdomains, the component of current normal to the plate edge in the solution of [21] vanishes prematurely in the subdomain nearest the edge.

Fig. 7 compares the calculated radar cross section (RCS) with the thin plate measurements of Kouyoumjian [22] and the computations of Rahmat-Samii and Mittra [23] for a square plate. In the latter case, we suspect that the premature vanishing of the current near the plate edge causes the underestimation in the RCS observed in the figure for lower frequencies. Kouyoumjian has also computed the RCS from a variational formula and we find no discernable difference between his computations and our results for square plates whose sides are smaller than  $0.4 \lambda$ , the range for which his formula should be most accurate. Also shown in Fig. 7 is a plot of the

<sup>3</sup> The data reported in [21] is actually for the electric field in a square aperture in a ground plane but has been converted to an equivalent electric current on a square conducting plate via the duality of the plate and aperture problems.

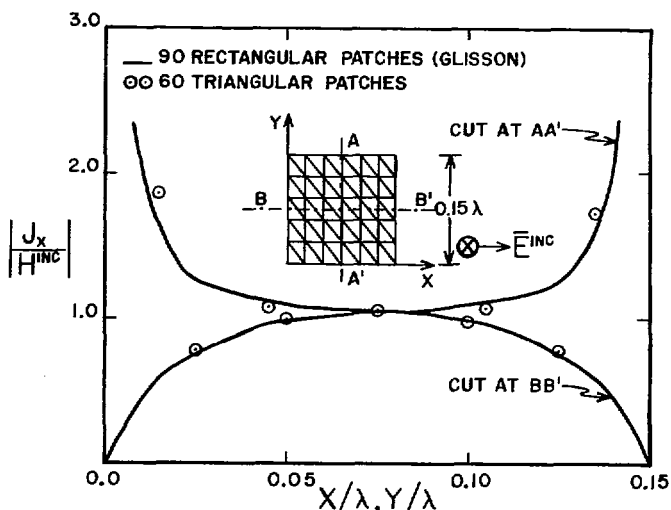


Fig. 5. Distribution of dominant component of current on  $0.15 \lambda$  square flat plate.

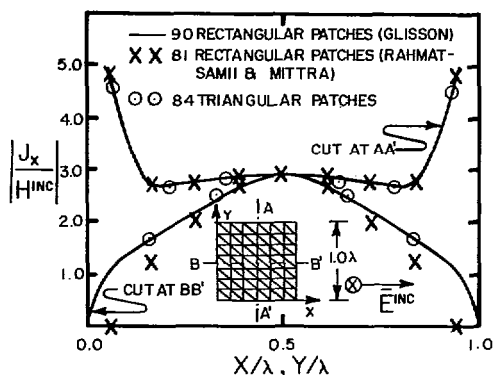


Fig. 6. Distribution of dominant component of current on  $1.0 \lambda$  square flat plate.

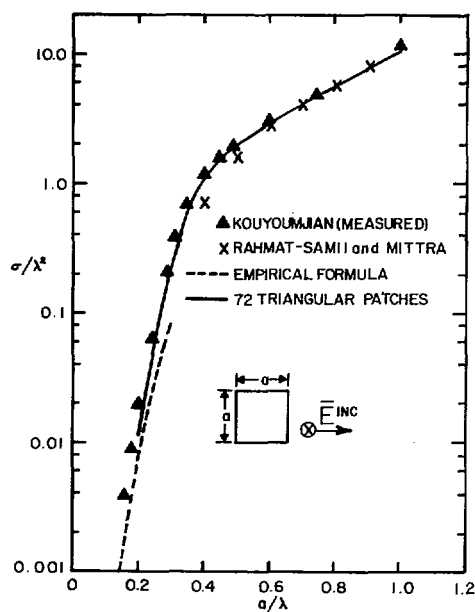


Fig. 7. Monostatic radar cross section versus frequency for square plate, normal incidence. Measurements are for plate of thickness  $0.000127 \lambda$ .

RCS for a square plate given by an empirical formula derived from measurements [24].

While there is generally very good agreement between the various results reported in Figs. 6 and 7, we have not been able to obtain a favorable comparison with the corresponding current distribution and RCS calculations of Wang *et al.* [7]. There are several reasons to suspect their calculations. First, they employ a set of basis functions which would generally cause spurious oscillations in the current distribution along the direction of current flow, and which would hence be expected to adversely affect the solution for the current distribution and, ultimately, the RCS. Secondly, their model ignores the presence of cross-polarized components of surface current on the plate. Finally, in the RCS case, the excellent agreement which they obtain between computed and measured radar cross section is unfortunately based on a comparison to the thick plate rather than the thin plate measurements of Kouyoumjian [22] for which their theory more appropriately applies and which we have shown in Fig. 7.

### Bent Plate

Fig. 8 shows the dominant component current distribution along a cut through the symmetry plane of a bent square plate. The bend is parallel to and located a distance of one-third the plate width from one edge, and a plane wave with the electric field polarized parallel to the bend is incident normal to the larger section of the bent plate. The smaller plate section is bent through an angle of  $50^\circ$  toward the shadow side of the plate. Other frequencies, polarizations, and angles of incidence have been examined, and the resulting current distributions show good correspondence with those of Glisson [16].

### Circular Disk

Fig. 9 shows the computed current distribution on a circular disk illuminated by a normally incident plane wave. The component  $J_\phi$  is shown along a diameter cut oriented perpendicular to the incident electric field vector. Also shown for comparison is the quasi-static solution valid at low frequencies [25].

### Sphere

Fig. 10 shows the computed current distribution along the principal cuts on a  $0.2 \lambda$  radius conducting sphere. The cases of axial and equatorial incidence are both considered in order to observe the influence of the triangulation scheme on the solution. Also shown for comparison is the exact eigenfunction solution. Results for both illuminations are in very good agreement with the exact solution.

Although we have not attempted to solve the sphere problem at frequencies near its cavity resonances, we expect the usual difficulties associated with the EFIE formulation at the internal resonance frequencies of closed bodies to arise. To alleviate the problem, one might make use of the present treatment of the EFIE operator in a formulation which combines it with the MFIE operator in such a way as to eliminate the singularity which is present in both operators alone [26].

### Computational Aspects

Table I summarizes data on the number of triangular patches, number of unknowns, and the computation time required on a Univac 1100/83 computer to generate the results of Figs. 5, 6, 8, and 10. The timing data for Fig. 6 were not re-

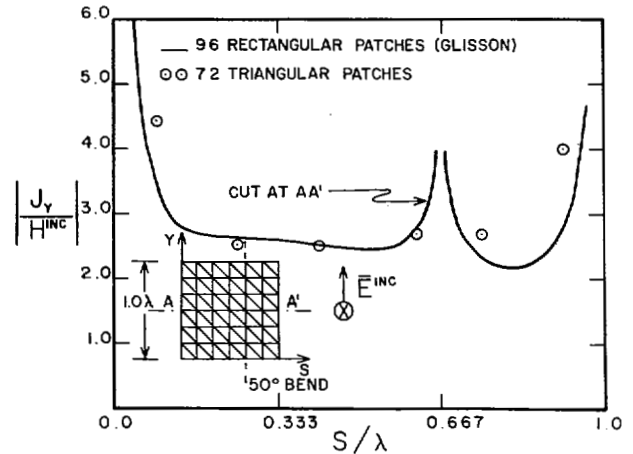


Fig. 8. Distribution of dominant component of current on  $1.0 \lambda$  bent square plate.

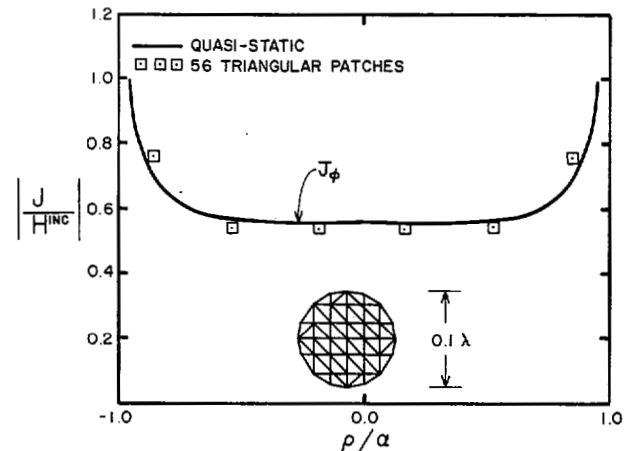


Fig. 9. Distribution of current on  $0.05 \lambda$  radius circular disk.

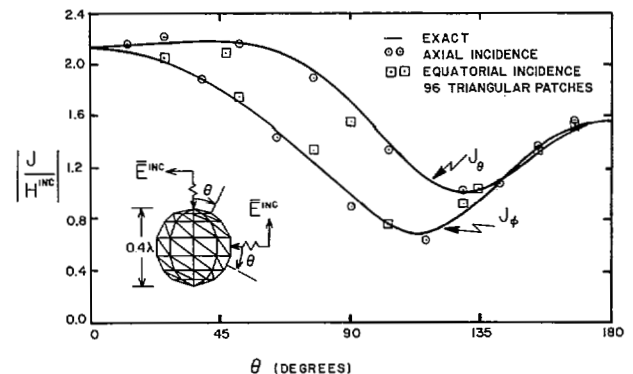


Fig. 10. Distribution of current components on  $0.2 \lambda$  radius conducting sphere.

TABLE I  
SUMMARY OF COMPUTATION DATA FOR SELECTED EXAMPLE PROBLEMS

Case (Figure Number)	Number of Patches $N_f$	Number of Boundary Edges $N_b$	Number of Unknowns $N^\dagger$	Matrix Fill Time (s)	Matrix Inversion Time (s)	Total CPU Time (s)
5	60	22	79	65	20	92
6	84	26	113	127*	57*	195*
8	72	24	96	94	35	139
10	96	0	144	163	118	294

\* Estimated from convergence study.

$\dagger N = (3N_f - N_b)/2$ .

corded during computation but are estimated from the convergence study discussed below. The present version of the computer code has not been completely optimized with respect to computation speed, and it should be possible to increase this speed by at least a factor of two or three by 1) decreasing the order of integration used to calculate the potential integrals when  $R^P$  in (34) is large compared to source patch size, and 2) replacing the matrix inversion procedure, used primarily for diagnostic purposes, by a linear equation solving procedure.

A convergence study of the current distribution on the  $1.0 \lambda$  square plate of Fig. 6 was carried out using 18, 32, 50, and 72 patches corresponding to 21, 40, 65, and 96 unknowns, respectively. It was found that, except for the nearly singular component of current nearest the plate edge, the computed currents in the sequence of computations differed from the results of Glisson (cf Fig. 6) by no more than 10 percent.

#### IV. SUMMARY

In this paper, the electric field integral equation (EFIE) is used with the method of moments to develop a simple and efficient numerical procedure for treating problems of scattering by arbitrarily shaped objects. For numerical purposes the objects are modeled by planar triangular surface patch models. Because the EFIE formulation is used, the procedure is applicable to both open and closed bodies. Crucial to the formulation is the development of a set of special subdomain basis functions which are defined on pairs of adjacent triangular patches and yield a current representation free of line or point charges at subdomain boundaries.

The approach is applied to the scattering problems of plane wave illumination of a flat square plate, a bent square plate, a circular disk, and a sphere. Comparisons of surface current density with previous computations or exact formulations show good correspondence in each case.

A listing of the computer code is available from the authors.

#### ACKNOWLEDGMENT

The authors are grateful to Mr. Robert Baxter and Dr. Deanne Pecora of the Lockheed Missiles and Space Company, Inc., for providing us with the results of their timing and convergence study summarized in Table I.

#### REFERENCES

- [1] J. H. Richmond, "A wire-grid model for scattering by conducting bodies," *IEEE Trans. Antennas Propagat.*, vol. AP-14, no. 6, pp. 782-786, Nov. 1966.
- [2] E. K. Miller and F. J. Deadrick, "Some computational aspects of thin-wire modeling," in *Numerical and Asymptotic Techniques in Electromagnetics*, R. Mittra, Ed. New York: Springer-Verlag, 1975, ch. 4.
- [3] K. S. H. Lee, L. Marin, and J. P. Castillo, "Limitations of wire-grid modeling of a closed surface," *IEEE Trans. Electromagn. Compat.*, vol. EMC-18, no. 3, pp. 123-129, Aug. 1976.
- [4] D. L. Knepp and J. Goldhirsh, "Numerical analysis of electromagnetic radiation properties of smooth conducting bodies of arbitrary shape," *IEEE Trans. Antennas Propagat.*, vol. AP-20, no. 3, pp. 383-388, May 1972.
- [5] N. C. Albertsen, J. E. Hansen, and N. E. Jensen, "Computation of radiation from wire antennas on conducting bodies," *IEEE Trans. Antennas Propagat.*, vol. AP-22, no. 2, pp. 200-206, Mar. 1974.
- [6] G. J. Burke and A. J. Poggio, "Numerical Electromagnetic Code (NEC) - method of moments," Naval Ocean Systems Center, San Diego, CA, Tech. Document 116, July 1977.
- [7] N. N. Wang, J. H. Richmond, and M. C. Gilreath, "Sinusoidal reaction formulation for radiation and scattering from conducting surfaces," *IEEE Trans. Antennas Propagat.*, vol. AP-23, no. 3, pp. 376-382, May 1975.
- [8] E. H. Newman and D. M. Pozar, "Electromagnetic modeling of composite wire and surface geometries," *IEEE Trans. Antennas Propagat.*, vol. AP-26, no. 6, pp. 784-789, Nov. 1978.
- [9] A. Sankar and T. C. Tong, "Current computation on complex structures by finite element method," *Electron. Lett.*, vol. 11, no. 20, pp. 481-482, Oct. 1975.
- [10] J. J. H. Wang, "Numerical analysis of three-dimensional arbitrarily-shaped conducting scatterers by trilateral surface cell modelling," *Radio Sci.*, vol. 13, no. 6, pp. 947-952, Nov.-Dec. 1978.
- [11] J. J. H. Wang and C. Papanicolaopolous, "Surface patch modeling of scatterers of arbitrary shapes," *Antennas Propagat. Soc. Int. Symp. Digest*, Univ. Washington, Seattle, WA, June 1979, pp. 159-162.
- [12] G. Jeng and A. Wexler, "Finite element, boundary integral equation analysis of scattering problems," *URSI Symp. on Electromagnetic Wave Theory*, Stanford Univ., Stanford, CA, June 1977, pp. 179-181.
- [13] J. Singh and A. T. Adams, "A non rectangular patch model for scattering from surfaces," *IEEE Trans. Antennas Propagat.*, vol. AP-27, no. 4, pp. 531-535, July 1979.
- [14] A. W. Glisson and D. R. Wilton, "Simple and efficient numerical methods for problems of electromagnetic radiation and scattering from surfaces," *IEEE Trans. Antennas Propagat.*, vol. AP-28, no. 5, pp. 593-603, Sept. 1980.
- [15] R. F. Harrington, *Field Computation by Moment Methods*. New York: Macmillan, 1968.
- [16] A. W. Glisson, "On the development of numerical techniques for treating arbitrarily-shaped surfaces," Ph.D. dissertation, Univ. Mississippi, 1978.
- [17] D. R. Wilton, S. S. M. Rao, and A. W. Glisson, "Electromagnetic scattering by arbitrary surfaces," Rome Air Development Center, Griffiss AFB, NY, Tech. Rep. RADC-TR-79-325, Mar. 1980.
- [18] J. Van Bladel, *Electromagnetic Fields*. New York: McGraw-Hill, 1964, p. 502.
- [19] O. C. Zienkiewicz, *The Finite Element Method in Engineering Science*. New York: McGraw-Hill, 1971.
- [20] P. C. Hammer, O. P. Marlowe, and A. H. Stroud, "Numerical integration over simplexes and cones," *Math. Tables Aids Comp.*, vol. 10, pp. 130-137, 1956.

- [21] C. M. Butler, Y. Rahmat-Samii, and R. Mittra, "Electromagnetic penetration through apertures in conducting surfaces," *IEEE Trans. Antennas Propagat.*, vol. AP-26, no. 1, pp. 82-93, Jan. 1978.
- [22] R. G. Kouyoumjian, "The calculation of the echo areas of perfectly conducting objects by the variational method," Ph.D. dissertation, The Ohio State Univ., 1953.
- [23] Y. Rahmat-Samii and R. Mittra, "Integral equation solution and RCS computation of a thin rectangular plate," *IEEE Trans. Antennas Propagat.*, vol. AP-22, no. 4, pp. 608-610, July 1974.
- [24] C. T. Ruck, Ed., *Radar Cross Section Handbook*. New York: Plenum, 1970, p. 523.
- [25] J. J. Bowman, T. B. A. Senior, and P. L. E. Uslenghi, *Electromagnetic and Acoustic Scattering by Simple Shapes*. Amsterdam: North-Holland, 1969, pp. 576-577.
- [26] J. R. Mautz and R. F. Harrington, "*H*-field, *E*-field, and combined field solutions for conducting bodies of revolution," *AEÜ*, vol. 32, no. 4, pp. 157-164, Apr. 1978.



**Sadasiva M. Rao** received the bachelor's degree in electrical and communications engineering from Osmania University, Hyderabad, India, in 1974, the master's degree from the Indian Institute of Sciences, Bangalore, India, in 1976, and the Ph.D. degree from the University of Mississippi, University, in 1980.

He is currently a Visiting Assistant Professor at the Department of Electrical Engineering, Rochester Institute of Technology, Rochester, NY. His research interests are in the areas of

electromagnetic theory and numerical methods applied to antennas and scattering.

**Donald R. Wilton** (S'63-M'65-M'70-SM'80), for a photograph and biography please see page 835 of the November 1981 issue of this TRANSACTION.



**Allen W. Glisson** (S'71-M'78) was born in Meridian, MS, on June 26, 1951. He received the B.S., M.S., and Ph.D. degrees in electrical engineering from the University of Mississippi, University, in 1973, 1975, and 1978, respectively.

From 1973 to 1978 he served as a Research Assistant in the Electrical Engineering Department of the University of Mississippi. In 1978, he joined the faculty of the University of Mississippi, where he is currently Assistant

Professor of Electrical Engineering. His current research interests include the development and application of numerical techniques for treating electromagnetic radiation and scattering problems.

Dr. Glisson is a member of Sigma Xi, Tau Beta Pi, Phi Kappa Phi, Eta Kappa Nu, and an associate member of Commission B of the International Union of Radio Science.